Amorphous $CaCO_3$: Influence of the formation time on its degree of hydration and stability

Huachuan Du[1], Mathias Steinacher[1], Camelia Borca[2], Thomas Huthwelker[2], Anna Murello[3], Francesco Stellacci[3] and Esther Amstad[1]*

1. Soft Materials Laboratory, Institute of Materials, École Polytechnique Fédérale de Lausanne (EPFL), 1015 Lausanne, Switzerland

2. Swiss Light Source, Paul Scherrer Institut, 5232 Villigen, Switzerland.

3. Institute of Materials, École Polytechnique Fédérale de Lausanne (EPFL), 1015 Lausanne, Switzerland

ABSTRACT: Calcium carbonate ($CaCO_3$) is one of the most abundant biominerals that is prevalent in rocks and often used as a structural material in marine animals. Many of these natural $CaCO_3$-based materials display excellent mechanical properties that are difficult to reproduce by man-made counterparts. This difficulty arises from the incomplete understanding of the influence of processing conditions on the structure and composition of $CaCO_3$. To gain a better understanding of the evolution of the structure and composition of amorphous $CaCO_3$ (ACC) particles during early stages, we introduce a new, organic solvent-free method that quenches this process with a high temporal resolution. We produce ACC particles inside small airborne drops that are formed with a microfluidic spray-dryer. These drops dry within 100 ms to 10 s and thereby arrest the formation of $CaCO_3$ particles on that timescale. Using the microfluidic spray-dryer, we demonstrate that the amount of mobile water contained in ACC particles increases with increasing formation time and hence with increasing particle size. As a result of the higher concentration of mobile water, larger particles are less stable against temperature-induced solid-state crystallization and electron beam-induced decomposition than smaller counterparts. The amount of mobile water contained in ACC can be substantially reduced, and hence their kinetic stability against solid-state transformations increased, if certain organic additives, such as poly(acrylic acid) (PAA), are incorporated. These insights might open up new opportunities to fabricate biomimetic $CaCO_3$-based materials with tunable structures and hence with properties that can be adapted to the needs of specific applications.

INTRODUCTION

Calcium carbonate is prevalent in nature for example as a geological mineral where significant amounts of CO_2 are stored,[1,2] or as biomineral that is an essential component of skeletons[3] and protective shells[4] of a wide variety of marine animals.[5] Nature produces $CaCO_3$-based materials that display remarkable mechanical[6] and optical properties[7] by closely controlling the structure, orientation, shape, and arrangement of the $CaCO_3$ crystals.[8,9] Inspired by these fascinating properties, a lot of work has been devoted to gaining a better understanding of the formation of $CaCO_3$ to produce bio-mimetic materials.[10–16] Natural[10,14,17–20] and synthetic[21–24] $CaCO_3$ crystals are typically formed from ACC particles that act as transient precursors. These precursors serve as a temporal storage of Ca^{2+} ions that, when needed, are transported to the desired location before being transformed into crystals with well-defined structures and morphologies.[14] The high level of control over the structure and therefore the properties of the resulting crystals achieved by nature is difficult to obtain in the laboratory. A contributing reason for this difficulty is the incomplete understanding of the influence of processing parameters on the formation and stability of ACC precursors.[25–29]

Synthesis conditions, such as the pH,[13,30] temperature,[31] and the drying method[32] have been shown to influence the formation pathways,[13] structure,[31,33] and stability[21,27,34] of ACC particles. The stability of ACC particles, that is directly related to their size,[25,35] is also influenced by the amount of water contained in them.[21,27,34] Whether the amount of water contained in ACC particles is influenced by the synthesis conditions remains to be determined. To experimentally study the influence of the synthesis conditions on the degree of hydration and the stability of ACC particles, the formation of ACC particles must be quenched at early stages with a temporal resolution of the order of milliseconds.[29] The formation of ACC is often quenched with organic solvents, such as ethanol, which $CaCO_3$ has a low solubility in.[21,34,36] The presence of these organic solvents influences the degree of hydration,[32,36,37] structural order,[38] stability,[39] and crystallization pathway[40] of ACC. Hence, the differentiation between effects that are inherent to ACC from those that have been induced by organic solvents is very difficult. Moreover, the time required to quench the formation ACC with this method is usually of the order of minutes.[41,42] Recently, some *in situ* liquid cell transmission electron microscopy (TEM)[41,43] and cryo-TEM[44,45] studies have been employed to investigate the early stages of $CaCO_3$ formation with a resolution down to a few seconds, although feasibility to achieve a resolution down to 100 ms has been shown.[46] The information that has been extracted from these measurements is limited to the size,

crystallinity, and morphology of particles. There are a few reports that employ TEM images to extract the degree of hydration of ACC particles from the image contrast. However, more systematic and direct studies on the influence of processing conditions on the composition of ACC particles including their degree of hydration remain elusive. To gain a better understanding of the correlation between processing conditions and the degree of hydration of ACC particles, it would be beneficial to establish a technique that quenches the formation of ACC during early stages without the need for organic solvents and without embedding them in a matrix that prevents further chemical analysis.

Here, we employ a microfluidic spray-dryer[47] to quench the formation of ACC particles at early stages by producing these particles in airborne aqueous drops that rapidly dry; this process does not require any organic solvents to quench the particle formation. To study the formation of ACC particles with a high temporal resolution, we vary the diameter of drops from 10 to 100 µm such that the formation time of ACC particles ranges from 100 ms to 10 s. We find that the amount of mobile water incorporated in ACC particles increases with increasing formation time and hence with increasing particle size. Because of the increased amount of mobile water, larger particles are less kinetically stable against temperature-induced crystallization and electron beam-induced decomposition than smaller counterparts. In line with these observations, we find that additives known to delay or even inhibit the crystallization of ACC, such as poly(acrylic acid) (PAA), reduce the mobility of water contained in ACC, thereby increasing their kinetic stability. These results indicate that the stability of ACC particles is directly related to the amount of mobile water contained in ACC particles. These insights offer new opportunities to tune the stability of ACC and thereby to facilitate its processing into biomimetic $CaCO_3$-based materials with tunable structures and hence with properties that can be adapted to the needs of the specific applications.

RESULTS

Production of ACC particles through spray-drying

We produce ACC nanoparticles with a poly(dimethyl siloxane) (PDMS)-based microfluidic spray-dryer[47] that is fabricated using soft lithography.[48] The spray-dryer contains two inlets for liquids and six inlets for gases, as schematically shown in **Figure 1a**. To avoid any influence of counter ions such as Na^+ and Cl^- on the structure and stability of spray-dried ACC particles,[21] we form them from an aqueous solution containing $Ca(OH)_2$ that is spray-dried using CO_2-enriched air: $Ca(OH)_2 + CO_2 = CaCO_3 + H_2O$. Aqueous drops containing $Ca(OH)_2$ form at the first liquid-gas junction and are sequentially accelerated by the air that is injected through the additional gas inlets 2-5. To ensure complete conversion of $Ca(OH)_2$ into $CaCO_3$, we enrich the air that is injected through the last gas inlet with 10 vol% CO_2. Drops exit the device though an outlet and are collected on a solid substrate located 20 cm apart where they are fully dried by the gas flow that exits the device. Because nanoparticles are deposited on the substrate before the drop is fully dried, they are well separated from each other even if many of them are formed in a single drop, as shown in the scanning electron microscopy (SEM) image in **Figure 1b**.

To test the influence of the formation time of ACC particles on their degree of hydration and the structure, we produce

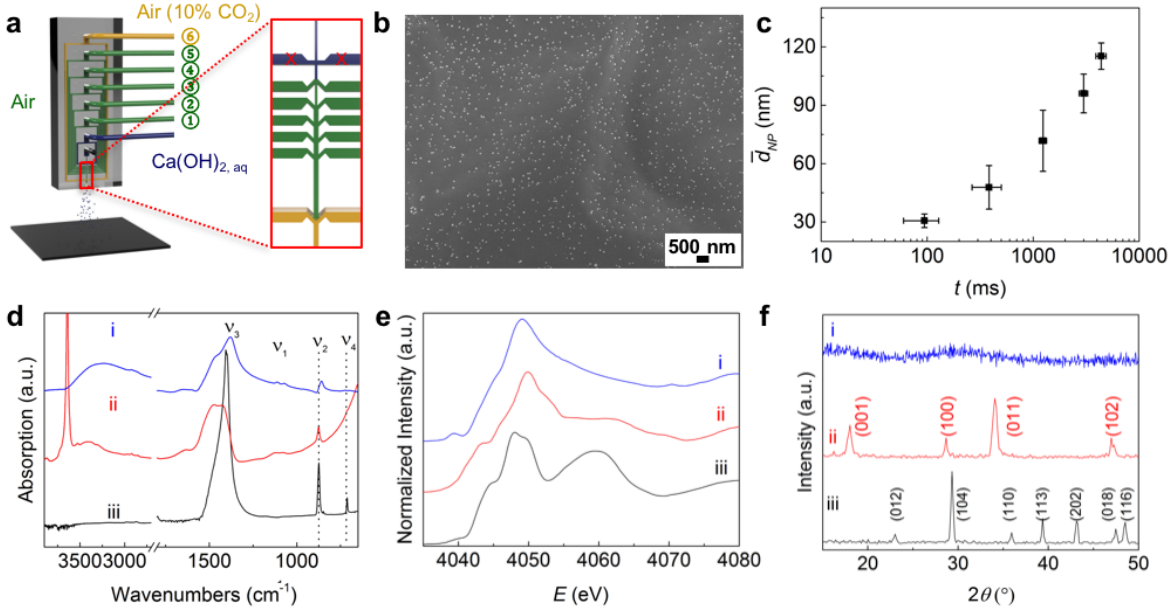

Figure 1. Production and characterization of amorphous $CaCO_3$ nanoparticles. (a) Schematic illustration of the microfluidic spray-dryer that contains two inlets for liquids (blue) whereof one is used to inject an aqueous solution containing $Ca(OH)_2$, and the other inlet is blocked. In addition, the microfluidic spray-dryer contains six inlets for air, five to inject unmodified air (green) and one to inject air enriched with 10% CO_2 (brown). (b) SEM image of the spray dried $CaCO_3$ nanoparticles. (c) Influence of the drying time of the drops (t), on the average diameter of spray-dried $CaCO_3$ nanoparticles ($\bar{d}_{NP}$). (d) FTIR, (e) Ca K-edge XANES and (f) XRD traces of spray dried $CaCO_3$ nanoparticles (blue, i) and reference traces of $Ca(OH)_2$ (red, ii) and calcite (black, iii). $Ca(OH)_2$ reference samples contain small amounts of calcite. The complementary results obtained from FTIR, XANES and XRD suggest that spray-dried particles are amorphous $CaCO_3$.

them in airborne drops with different sizes. Drops with a diameter of 10 µm dry within 100 ms whereas 100 µm diameter drops dry within 10 s, as described in the **Supporting Information**. This drying time is directly related to the time during which ACC particles can form inside drops: particles can start to form when the solute concentration exceeds its saturation concentration and their formation is quenched when the drop is fully dried. We approximate the particle formation to be initiated when drops exit the device where they are exposed to higher concentrations of CO_2 such that the formation time of particles is very similar to the drying time of drops. If we vary the formation time of the particles, t, from 100 ms to 10 s, the average diameter of the resulting particles, $\overline{d}_{NP}$, increases from 30 nm to 120 nm, as shown in **Figure 1c**. Similar behaviors of particles growing with time has been observed by other experimental techniques. Using this correlation, we can deduce the formation time of particles by quantifying their size and thereby study early stages of the formation of ACC particles with a high temporal resolution without the need for any organic solvent.

Drops produced in the microfluidic spray-dryer dry quickly such that the time available for the formation of ACC particles is very short. To test if this time is sufficient to fully convert $Ca(OH)_2$ into $CaCO_3$, we characterize spray-dried particles using Fourier-transform infrared spectroscopy (FTIR). The spray-dried particles do not display any sharp absorption band at 3640 cm^{-1} that corresponds to the OH^- stretch vibration and is prominent in the reference trace of $Ca(OH)_2$, as shown in **Figure 1d**. This result suggest that spray-dried particles do not contain significant amounts of $Ca(OH)_2$. Instead, spray-dried particles display an absorption band at 863 cm^{-1} corresponding to the out-of-plane bending vibration of CO_3^{2-} (v_2) and they do not show any band around 712 cm^{-1} that would correspond to the in-plane bending vibration of CO_3^{2-} (v_4). The location of the v_2 band and the absence of the v_4 band measured for the spray-dried sample is characteristic for ACC.[49–52] Hence, our FTIR results suggest that $Ca(OH)_2$ is fully converted into ACC during the spray-drying process. The FTIR spectrum of spray-dried particles also displays a broad absorption band in the region of 2750–3600 cm^{-1} and a small band around 1640 cm^{-1}; these bands are characteristic for water contained in ACC,[49,50] suggesting that spray-dried particles contain significant amounts of water. To confirm the structure and composition of spray-dried particles, we perform X-ray absorption (XAS) measurements on the Ca K-edge and compare the spectrum measured for spray-dried particles to the reference spectra of calcite, the most stable crystalline form of $CaCO_3$ at room temperature and ambient conditions, and $Ca(OH)_2$. The spray-dried particles display a small pre-edge peak at 4040 eV and a single peak at the absorption edge of 4049 eV, in stark contrast to the reference spectra, as shown in the X-ray absorption near edge structure (XANES) spectrum in **Figure 1e**. The XANES spectrum of spray-dried particles indicates the particles are composed of ACC, in good agreement with previously reported results for ACC particles produced in bulk.[52–55] A fit of the extended X-ray absorption fine structure (EXAFS) region reveals that the distance of the first oxygen coordination shell around calcium (R) is 2.4 ± 0.04 Å and the coordination number (N) is 6.4 ± 3.3, as detailed in **Figure S2**. No more distant shells are observed, suggesting that our particles are amorphous, well in agreement with our FTIR and XANES results. Our EXAFS results agree well with those reported for ACC particles that have

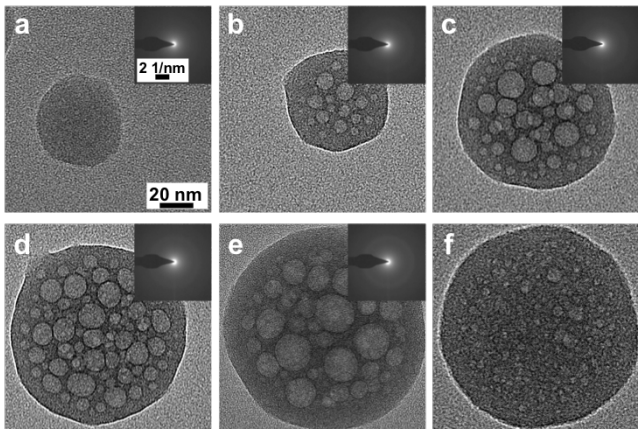

Figure 2. Influence of particle size. TEM images of ACC particles with a diameter of (a) 47 nm, (b) 65 nm, (c) 97 nm, (d) 112 nm and (e) 130 nm with the SAED patterns as insets. (f) TEM image of a 130 nm diameter ACC particle that has been stored in a desiccator under reduced pressure for 2 months.

been produced in bulk,[53,55] providing evidence that the spray-dried ACC particles possess a similar short-range order. To further confirm the amorphous structure of spray-dried particles, we perform X-ray diffraction (XRD) on the samples. In agreement with our previous results, we do not observe any sharp diffraction peak in the XRD trace of the spray-dried sample, in stark contrast to the reference samples, as shown in **Figure 1f**.

Influence of the formation time on the degree of hydration in ACC particles

To investigate the influence of the formation time of spray-dried ACC particles on their morphology, we visualize them using transmission electron microscopy (TEM). To minimize the risk for electron beam-induced changes in the morphology of the spray-dried particles while they are imaged, we acquire images with a relatively low, well-defined electron dose of 60 $e \cdot Å^{-2} \cdot s^{-1}$. When imaged under these conditions, the morphology of particles changes only minimally during a 100 s long exposure, as shown in **Movie S1**. The acquisition time of a TEM image is much shorter, approximately 10 s, and therefore we assume the morphology of particles to remain unchanged during the image acquisition. Spray-dried $CaCO_3$ particles do not display any diffraction spots in their selected area electron diffraction (SAED) patterns, as exemplified in the insets of **Figure 2a** to **Figure 2e**. Instead, the SAED pattern consists of diffuse rings, further confirming the amorphous structure of the particles, well in agreement with our FTIR, XAS, and XRD results. However, particles with varying sizes show distinctly different morphologies: while particles with diameters below 50 nm have a uniform contrast, larger particles contain electron-light domains that are embedded in an electron-dense matrix. The number and average size of the electron-light domains increase with increasing particle size, as shown in **Figures 2a-e**. To exclude that this morphology is related to the composition of the reactants used to

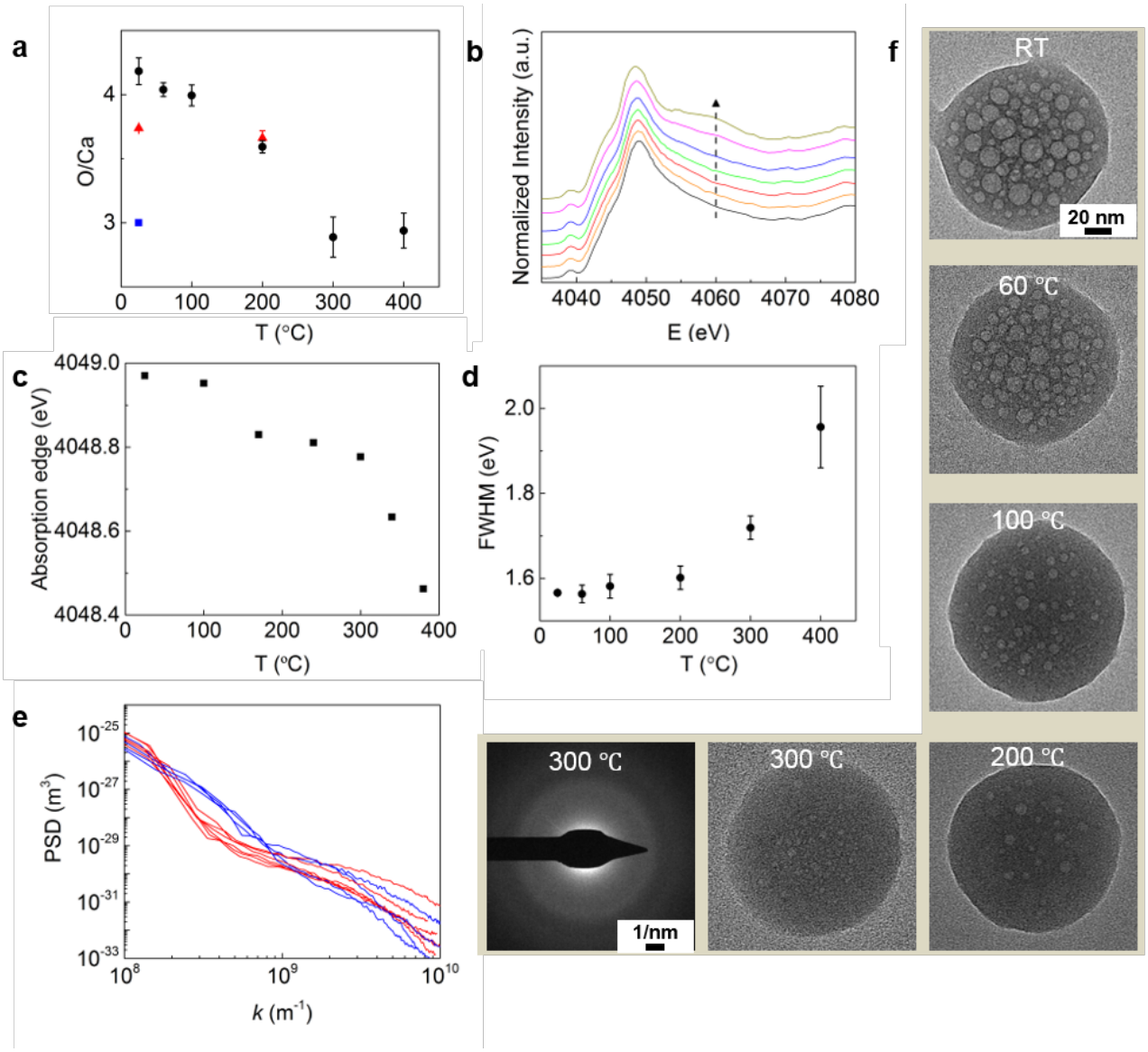

Figure 3. Influence of the degree of hydration of ACC particles. (a) Atomic ratio of O to Ca (O/Ca) of ACC particles with an average diameter of 130 nm (●) and those with an average diameter of 30 nm (▲), as a function of the annealing temperature, as well as a calcite reference sample (■), as quantified from XPS measurements. These results indicate that larger ACC particles are more hydrated than smaller counterparts. (b) Ca-K edge XANES spectra and (c) the corresponding positions of the absorption edge of ACC particles with an average diameter of 130 nm that are heated *in situ* to different temperatures. Following the direction of arrow, the temperature is increased from room temperature (RT) to 100 °C, 170 °C, 240 °C, 300 °C, 340 °C and 380 °C. The results indicate that structural water is lost at temperatures exceeding 170°C. (d) Full width half maximum (FWHM) of the Ca $2P_{3/2}$ peaks of ACC particles with an average diameter of 130 nm as a function of the annealing temperature, as determined with XPS. (e) Power spectral density (PSD) plots of the freshly produced (blue) particles and those annealed at 200 °C for 3 h (red) calculated from the AFM images. The annealed particles have a significantly lower PSD than the as-prepared ones in a spatial frequency (k) ranging from 2×10^8 to 10^9 m^{-1} that corresponds to features with a size of 6-30 nm in real space. These results indicate that the number of 6-30 nm sized features on the surface of particles significantly decreases upon annealing. The measurement has been repeated on different particles, each represented by one curve in the figure. (f) TEM images and SAED pattern of 130 nm diameter ACC particles that have been annealed at different temperatures.

produce ACC particles, we co-spray dry an aqueous solution containing $CaCl_2$ with one containing Na_2CO_3. The resulting ACC particles display a very similar morphology, as shown in **Figure S3**, indicating that this morphology is inherent to our ACC particles. Transmission electron microscopy images of ACC particles that display two distinctly different phases[21,32,36] as well as those with a homogeneous contrast[56,57] have been reported. The origin of these differences in morphology is not yet fully understood. A possible reason for these abrupt changes in contrast within a single particle is radiolysis, where the electron beam ionizes water contained in ACC particles and converts it into gases.[58] The resulting gases are trapped within the particles and form pores that correspond to the electron-light regions.[21,57] In this case, the electron beam-induced phase separation could be taken as a qualitative measure for the degree of hydration of the ACC particles. Our results would then suggest that the propensity of particles to undergo electron beam-induced phase separation in-

creases with increasing degree of hydration. To test this suggestion, we store spray-dried ACC particles in a desiccator at reduced pressure for two months to remove parts of the water contained in as-prepared ACC particles.[59] Indeed, these dried particles display much smaller electron-light regions than as-prepared particles with similar diameters, as a comparison between **Figure 2e** and **Figure 2f** reveals. These results suggest that the observed phase separation is related to the degree of hydration of the particles. Hence, we conclude that small particles, whose formation is quenched at earlier stages, are less hydrated than their larger counterparts. Our TEM results indicate that the degree of hydration increases with increasing formation time and hence, with increasing particle size. To test this suggestion, we quantify the amount of water contained in spray-dried ACC particles using X-ray photoelectron spectroscopy (XPS). XPS only probes the surface of particles. However, because the TEM images do not provide any evidence for core-shell structures of our particles, as shown in **Figure 2,** we approximate the surface composition of the particles to be equal to that of their cores. Using this approximation, we quantify the amount of water contained in particles with an average diameter of 130 nm, whose formation time is 10 s. Similarly, we quantify the amount of water contained in particles with an average diameter of 30 nm, whose formation time is 100 ms. The molar amount of water contained in 30 nm diameter particles is 30 % lower than that contained in larger particles, as indicated by the lower atomic ratio of O to Ca, shown in **Figure 3a** and described in the **Supporting Information**. This result indicates that the degree of hydration of spray-dried ACC particles increases with increasing formation time and supports our TEM results. The correlation between the formation time and the amount of mobile water contained in ACC particles might be a contributing reason for the wide range of degrees of hydrations that have been reported for particles produced under similar conditions, where molar ratios of H_2O to $CaCO_3$ vary from 0.4 to 1.58.[21,34,53,60,61]

Mobility of water contained in ACC particles

Our results suggest that larger ACC particles possess a higher degree of hydration. This water is well-known to influence the stability of ACC particles but the extent of its effect depends on its interaction with $CaCO_3$.[62–64] Water contained in ACC can weakly interact with CO_3^{2-} and therefore possess a high mobility.[53,65–67] Water can also strongly interact with Ca^{2+} ions such that it has a restricted mobility and is considered to be structural water.[53,65–67] This strongly bound water is an integral part of the structure of ACC, such that its loss is accompanied by a re-arrangement of Ca^{2+} and CO_3^{2-}.[26,62] Because of the stronger interatomic interactions, structural water evaporates at much higher temperatures than mobile water does.[26,36] To test if spray-dried 130 nm diameter ACC particles contain any structural water, we acquire XANES spectra as a function of the temperature that is varied *in situ*. When the temperature is increased above 170 °C, a shoulder around 4060 eV appears and the position of the absorption edge is shifted towards lower values, as summarized in **Figure 3b and Figure 3c**. These results hint at a re-arrangement of the ions that occurs upon removal of structural water. In line with these observations, the full width half maximum (FWHM) of the Ca $2P_{3/2}$ peak measured with XPS increases significantly if the particles are annealed at temperatures above 200°C, as shown in **Figure 3d**. These results indicate that ion re-arrangement occurs both, in the core and at the surface of the particles.

If a large fraction of ions located in proximity to the surface re-arranges, we expect the surface roughness of these particles to change. To test this expectation, we image the surface of these particles with atomic force microscopy (AFM) before and after they have been annealed at 200 °C for 3 h. Indeed, a comparison of the power spectral density function (PSDF) analysis performed on the AFM images reveals that annealed particles have a considerably smoother surface than the as-produced counterparts, as shown in **Figure 3e**. These results indicate that structural water is removed around 200 °C and this removal is accompanied by a re-arrangement of the ions contained in ACC.

Our results suggest that spray-dried particles encompass a significant amount of structural water. To quantify the amount of structural water, we measure the O/Ca ratio of the particles as a function of the annealing temperature using XPS. Particles with diameters around 130 nm contain approximately 1.2 H_2O molecule per $CaCO_3$. Approximately 50% of this water is removed below 200 °C, whereas the remaining water is removed between 200 °C and 300 °C, as summarized in **Figure 3a**. These results suggest that about 50% of the water contained in 130 nm diameter particles is structural water, corresponding to a concentration of 0.6 molecules of structural H_2O per $CaCO_3$. Remarkably, this concentration is very similar to the total amount of water contained in 30 nm diameter ACC particles, suggesting that the majority of water contained in these small particles is structural. To test this suggestion, we quantify the degree of hydration of 30 nm diameter particles that have been annealed at 200°C. Indeed, the degree of hydration of 30 nm diameter particles does not measurably change upon annealing at 200°C for 3 h, as shown in **Figure 3a**. These results indicate that the vast majority of water contained in smaller particles is structural. The very low concentration of mobile water contained in 30 nm diameter particles likely renders them more stable against radiolysis, as shown in **Figure 2a**. To test if it is indeed the amount of mobile water contained in ACC particles that determines their susceptibility towards radiolysis and not their size, we visualize larger particles that have been annealed at different temperatures using TEM. While particles with a diameter of 130 nm that have been annealed at 100°C or below undergo considerable electron beam-induced phase separation, particles annealed at 200 °C or above only contain very few electron-light domains, as shown in **Figure 3f**. These results confirm that the presence of mobile water renders particles prone to undergo electron beam-induced phase separation. Moreover, these results suggest that the observed increase in the degree of hydration with increasing size of the ACC particles is mainly attributed to the increasing amount of mobile water.

Influence of mobile water on the stability of ACC particles

The electron beam is known to decompose $CaCO_3$ into crystalline CaO and CO_2, if its intensity is sufficiently high.[68] If ACC particles are imaged with a low dose of electrons, 60 $e \cdot Å^{-2} \cdot s^{-1}$, we do not observe any formation of CaO. However, we expect the particles that contain a high concentration of mobile water and hence that undergo radiolysis even if exposed to a low electron dose, to also be prone to an electron beam-induced decomposition. To test our expectation, we expose particles to a high electron dose of approximately 400 $e \cdot Å^{-2} \cdot s^{-1}$ and observe structural changes *in situ*. In 130 nm diameter particles that contain significant amounts of mobile

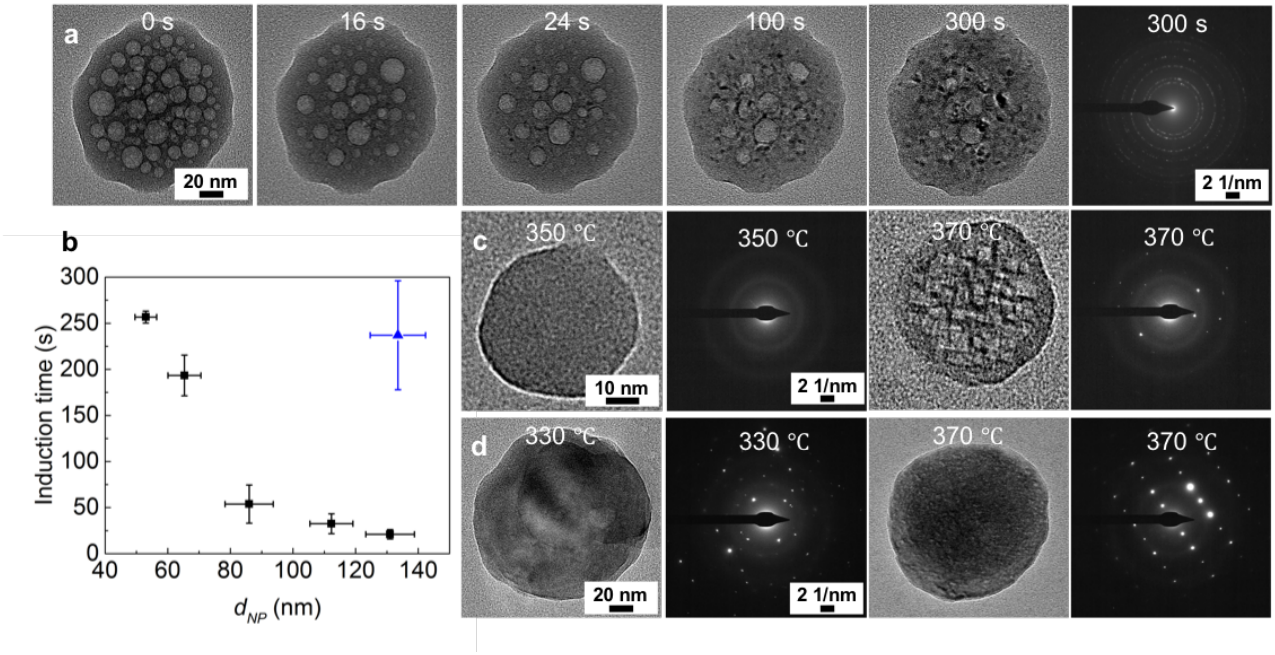

Figure 4. Stability of ACC particles against electron beam-induced decomposition and temperature-induced crystallization. (a) Time-lapse TEM images and SAED pattern of a 130 nm diameter ACC particle exposed to a focused electron beam with a dose of 400 e·Å^{-2}·s^{-1}. (b) Influence of the diameter (d_{NP}) of as-prepared ACC particles (■) and those dehydrated in vacuum (▲), on the exposure time required to induce the formation of CaO crystals. (c, d) TEM images and SAED patterns of (c) 45 nm and (d) 130 nm diameter ACC particles that have been annealed at different temperatures. These results indicate that particles that have been partially dehydrated are less prone to undergo electron beam-induced decomposition.

water, the electron-light domains rapidly grow and coalesce before small crystals start to form at the interface of the domains, as illustrated in time-lapse TEM micrographs of **Figure 4a** and in **Movie S2**. The crystals that form at the interface and grow into the electron-dense phase are composed of CaO, as indicated by the diffraction pattern in **Figure 4a**. The illumination time required to induce this decomposition increases with decreasing particle size, as summarized in **Figure 4b**.

This result suggests that the time required to induce the decomposition of ACC into CaO scales inversely with the amount of mobile water contained in ACC. To confirm this suggestion, we dehydrate the ACC particles in vacuum or by annealing them at 300 °C and subsequently expose them to a focused electron beam. The dehydrated particles are significantly more stable than as-produced counterparts with a similar average diameter, as shown in time-lapse TEM micrographs in **Figure S6** and summarized in **Figure 4b**. These results confirm that the stability of ACC particles against electron beam-induced decomposition increases with decreasing amount of mobile water.

The stability of ACC particles against crystallization depends on the degree of hydration.[21,27] However, it is unclear if this stability depends on the amount of mobile or structural water. To study the influence of the amount of mobile water on the stability of spray-dried particles, we anneal particles with an average diameter of 45 nm and those with an average diameter of 130 nm in a furnace and quantify the temperature where temperature-induced crystallization occurs using TEM. ACC particles with a diameter of 130 nm start to crystallize at 330 °C whereas those with a diameter of 45 nm that contain only a very small fraction of mobile water start to crystallize at a significantly higher temperature, 370 °C, as shown in the TEM images and SAED patterns in **Figure 4c** and **Fig 4d**. These results indicate that the temperature where ACC particles start to crystallize decreases with increasing amount of mobile water. Because the amount of mobile water in our ACC particles increases with increasing size, the temperature where particles start to crystallize decreases with increasing size, well in agreement with previous reports on ACC particles produced in bulk.[51] Our results suggest that this decrease in the crystallization temperature measured for particles whose diameter increases from 30 – 130 nm is related to their change in composition, the increased degree of hydration, rather than being purely a size effect.

The concentration of mobile water contained in ACC particles determines their stability against temperature-induced crystallization. Interestingly, the concentration of mobile water contained in ACC particles also influences the size of the resulting crystals: The size of grains formed in 45 nm diameter particles is much smaller than that of grains formed in 130 nm diameter particles, as shown in **Figure 4c** and **Figure 4d**. Indeed, 130 nm particles often transform into a single crystal whereas 45 nm diameter particles are transformed into polycrystals. We attribute this difference to the mobility of the ions: larger particles contain a higher amount of mobile water that likely enhances the mobility of Ca^{2+} and CO_3^{2-}. The higher mobility allows nuclei to grow relatively quickly and consume the ions before many more nuclei can form. By contrast, the mobility of Ca^{2+} and CO_3^{2-} contained in smaller particles, that contain less mobile water, is likely lower such that the crystals grow much slower and many more nuclei can form before all the ions contained in ACC are consumed.

Influence of poly(acrylic acid) on the stability of ACC particles

The formation of ACC particles[69,70] and their stability against crystallization[71–74] strongly depend on the additives contained

in them. To test if additives influence the amount of mobile water contained in ACC particles, we produce ACC particles that are functionalized with poly(acrylic acid) (PAA) through co-spray-drying; poly(acrylic acid) is known to delay the crystallization of ACC[46,69,70,72] without measurably altering its degree of hydration.[72] The spray-dried PAA-functionalized particles are significantly smaller than additive-free counterparts and individual particles are interconnected by PAA, as detailed in **Figure S7**. The most striking difference between PAA-functionalized and additive-free particles is their stability against electron beam-induced phase separation: PAA-functionalized particles with diameters up to 100 nm do not undergo electron beam-induced phase separation, in stark contrast to additive-free counterparts with similar sizes, as shown in **Figure 5a**. This result indicates that the water contained in PAA-functionalized particles is less mobile, likely because it strongly interacts with PAA.[75] This behavior is similar to that observed for other additives, such as poly(sodium styrenesulfonate),[75] Mg^{2+},[50] and PO_4^{3-}.[76] As a result of the lower mobility of water contained in ACC, these particles are more stable against electron beam-induced decomposition: PAA-functionalized particles with a diameter of 100 nm do not undergo any decomposition even if exposed to a focused electron beam for 280 s, which is six times longer than the time required to induce decomposition of additive-free particles of a similar size, as shown in **Figure 5b**. Similarly, PAA-functionalized particles are more stable against temperature-induced crystallization: these particles do not crystallize even if exposed to 370 °C for 3 h although they undergo a noticeable change in morphology, as shown in **Figure 5c**, well in agreement with results reported for particles produced in bulk.[72] We assign the higher stability of PAA-functionalized particles again to the lower mobility of water that results in an increased free energy barrier for crystallization.[36]

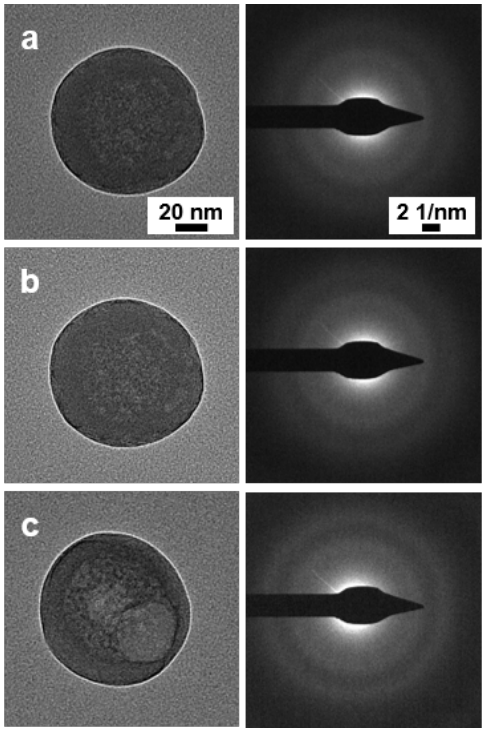

Figure 5. PAA-functionalized ACC particle. (a-b) TEM images (left) and SAED patterns (right) of a 100 nm diameter PAA-functionalized ACC particle (a) as-produced and (b) after having been exposed to a focused electron beam with a dose of 400 $e \cdot Å^{-2} \cdot s^{-1}$ for 280 s indicate that these particles are less prone to undergo electron beam-induced changes in their morphology. (c) TEM image and SAED patterns of a PAA-functionalized ACC particle after having been annealed at 370 °C for 3 h.

DISCUSSION

Molecular dynamics simulations predict water to play a key role in the formation of ACC particles.[25,77] They show that the enthalpy of ACC particles decreases with increasing degree of hydration,[25,62,64] in good agreement with calorimetric measurements.[30,59] However, the incorporation of water into ACC reduces the total entropy of the ACC-H_2O system with respect to the aqueous solution and it is still unclear whether the enthalpy or entropy term dominates the formation and growth of ACC.[25,59,64] Our results indicate that with increasing particle size from 30 to 130 nm, the amount of mobile water increases. As a result, the enthalpy of the system decreases during the growth of ACC. While the precise estimation of entropy penalty that results from the incorporation of water into ACC is complicated and ambiguous,[25,59,64] we expect the entropy penalty due to incorporation of mobile water to be smaller than that for structural water and thereby it can be negligible. Hence, the increased amount of mobile water that increases with increasing particle size reduces the free energy of the system, rendering the ACC growth thermodynamically favorable, as schematically illustrated in **Figure 6**.

To transform ACC particles into crystals that do not possess water, water contained in ACC must be expelled.[21,23,36,78] If put in bulk solutions at room temperatures and ambient pressures, ACC particles dissolve and recrystallize from a supersaturated solution.[80] By contrast, if high temperature or high pressure[27] is applied without the presence of bulk water or high relative humidity, ACC particles crystallize through solid-state transformation. As we transform ACC particles into crystals by annealing them at elevated temperature, we expect the crystallization goes through solid-state transformation. During the solid-state transformation, the hydrated ACC dehydrates into anhydrous one prior to the secondary nucleation by the re-arrangement of Ca^{2+} and CO_3^{2-} among the amorphous matrix. This is in good agreement with our observation in **Figure 3**. Moreover, at a temperature of 300 °C that is slightly below the critical crystallization temperature, where most of water contained in particles have been removed, no crystals caused by ACC dissolving and recrystallizing are present. Hence, this confirms that ACC particles undergo solid-state transformation when they are annealed at higher temperatures.

It has been shown the dehydration process is endothermic,[59,62] while the transformation from anhydrous ACC to crystals is exothermic. As a result, the kinetics of ACC crystallization and therefore its stability is more controlled by the free energy barrier of dehydration step in the solid-state transformation. An increasing amount of mobile water contained in larger particles likely decreases the free energy barrier through increasing the mobility of Ca^{2+} and CO_3^{2-} ions and hence facilitates their re-arrangement.[26,59] Hence, larger particles are less stable against solid-state transformation, well in agreement with our experimental results. By contrast, if ACC particles crystallize via dissolution and recrystallization in bulk solutions at room temperatures and pressures,[80] this process is thermodynamically favorable since the dissolution is exothermic. As a result, the dissolution and crystallization rate are less affected by the

amount of mobile water but mass transport. Due to a higher surface/volume ratio, smaller particles are expected to dissolve and crystallize much faster than larger particles, which well supports the reported results for ACC particles that have been produced with bulk method.[51] To sum up, the different factors that govern the kinetics of crystallization performed in bulk solution and through solid-state transformation might be the reason why small particles are more stable against solid-state transformation than larger ones but less stable against crystallization in solution.

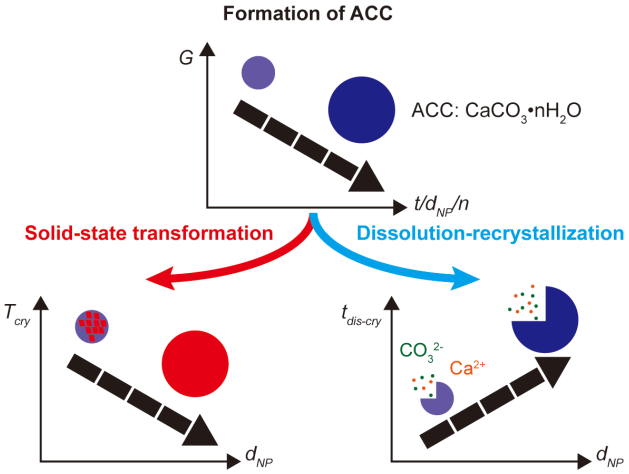

Figure 6. Schematic illustration of the growth of ACC particles and their transformation into crystals. The free energy (G) of ACC particles decreases with increasing formation time (t), particle diameter (d_{NP}), and degree of hydration (n). ACC particles can transform into crystals through solid-state transformation (left) or dissolution-recrystallization (right). If crystallized through a temperature-induced solid-state transformation, the crystallization temperature (T_{cry}) decreases with increasing particle size and hence with increasing amount of mobile water contained in ACC particles. By contrast, if crystallized through dissolution-recrystallization, the time required for crystals to form ($t_{dis\text{-}cry}$) increases with increasing particle size and hence with increasing amount of mobile water contained in them.

CONCLUSION

The microfluidic spray-dryer quenches reactions through rapid drying of the aqueous solution without the need for organic solvents. Thereby, it enables studying early stages of the formation of ACC particles with a high temporal resolution. We demonstrate that the amount of mobile water contained in ACC particles increases with increasing formation time and hence, with increasing particle size. The amount of mobile water contained in these particles influences their kinetic stability against temperature-induced solid-state transformation and electron beam-induced decomposition. While we investigated the role of water in the formation and transformation of $CaCO_3$, our findings are not limited to this material but most likely also apply to the formation of many other materials that form via transient precursors, such as calcium phosphate, calcium oxalate, or calcium sulfate. Hence, our results enable the development of processes that offer a superior control over the degree of hydration and thus over the stability of transient precursors. Thereby, they might open up new possibilities to fabricate ceramic-based composites with a much tighter control over their structure and therefore over their properties. This will facilitate the fabrication of functional materials whose structures and properties more closely resemble those of natural counterparts.

EXPERIMENTS

Preparation of solution

All reagents are used as received. A saturated solution of $Ca(OH)_2$ (~23 mM) is prepared by adding 2 g $Ca(OH)_2$ (ACS reagent, ≥95.0%, Sigma-Aldrich) in 1 L deionized water (Direct-Q®, Merck Millipore, 25 °C) and stirring overnight. To avoid the formation of $CaCO_3$ precipitates, we degas the water over night using N_2. This solution (pH~12.6) is filtered through a 0.2-µm syringe filter (CH-PTFE-20/25, HROMAFIL® Xtra) and diluted to 2 mM (pH~11.6) before the experiment. To produce PAA-functionalized ACC particles, we add poly(acrylic acid) (PAA, Mw ~100,000 Da, 35 wt. % in H_2O, Sigma-Aldrich) with a concentration of 50 µg·mL^{-1} to the solution containing 2 mM $Ca(OH)_2$. To test the influence of the counterion to the Ca^{2+} and CO_3^{2-} ions used to produce $CaCO_3$ particles, we employ an aqueous solution containing 4 mM calcium chloride (≥98 %, anhydrous, Carl Roth) and one containing 4 mM sodium carbonate (ACS reagent, ≥99.5 %, anhydrous, Carl Roth).

Production of spray-dried ACC nanoparticles

We employ a PDMS-based microfluidic spray-dryer that contains two inlets for liquids and six inlets for gases, as has previously been published.[47] The spray-dryer is made of poly(dimethylsiloxane) (PDMS, Sylgard 184, Dow Corning) using soft lithography.[48] To make the channels non-wetting for the water drops, the surfaces of the channels are treated with dodecane (≥99.0%, ABCR) containing 5 vol% trichlorododecylsilane (≥95.0%, Sigma-Aldrich). Drops form at the first liquid-gas junction and are sequentially accelerated by the gas that is injected through the additional gas inlets. They are collected on a solid substrate and subsequently fully dried by the gas flow that exits the microfluidic spray-dryer.

To avoid any influence of counter ions such as Na^+ and Cl^- on the structure and stability of spray-dried particles, we produce them from an aqueous solution containing $Ca(OH)_2$ and expose it to CO_2. We inject an aqueous solution containing 2 mM $Ca(OH)_2$ into the first liquid inlet at a flow rate of 1 ml·h^{-1} using a syringe pump (Cronus Sigma 1000, Labhut). The second liquid inlet is included for flexibility and blocked for these experiments. To prevent precipitation reactions prior to drop formation, we form airborne drops containing $Ca(OH)_2$ using air. Drops are accelerated in the main channel by introducing additional air through inlets 2-5. To ensure complete conversion of $Ca(OH)_2$ into $CaCO_3$, the air injected through the last inlet is enriched with 10 vol% CO_2 that is produced by a gas mixer (KM60-2ME, Witt). We keep the pressure at all the air inlets constant at 0.3 MPa. Drops are collected on a silicon wafer or a carbon-coated TEM grid located 20 cm apart from the outlet of the device. After drops are fully dried by the gas flow existing the device, the solid particles are characterized.

To produce PAA-functionalized particles, we inject an aqueous solution containing 50 µg·mL^{-1} PAA and 2 mM $Ca(OH)_2$ and operate the device under same conditions. To produce ACC particles from aqueous solutions containing $CaCl_2$ and Na_2CO_3, we inject an aqueous solution containing 4 mM $CaCl_2$ at 0.5 mL·h^{-1} into the first liquid inlet and the second aqueous solution containing 4 mM Na_2CO_3 at 0.5 mL·h^{-1} into

the second liquid inlet. in this case, all 6 gas inlets are supplied with pure air.

As references, calcite powder (ACS reagent, ≥99.0%, Sigma-Aldrich) and calcium hydroxide (ACS reagent, ≥95.0%, Sigma-Aldrich) are used as received.

Dehydration of spray-dried ACC nanoparticles

We use thermal annealing and vacuum drying to dehydrate the ACC particles. Particles that are deposited onto TEM grids are heated in a nitrogen atmosphere using a Thermogravimetry Analysis 4000 (Perkin Elmer) at a rate of 10 °C·min^{-1} before they are kept at the desired temperature for 3 h. Particles that are deposited onto a silicon wafer are annealed in the muffle furnace (France-Etuves) at the desired temperature for 3 h. Particles that are dehydrated in vacuum are kept in a vacuum desiccator (VWR) for 2 months.

Characterizations

Scanning electron microscopy (SEM)

The size of ACC particles is characterized using Zeiss Merlin field emission SEM operated at an acceleration voltage of 6 kV and a probe of 100 pA. To avoid charging of the samples, they are coated with a 4 nm thick iridium film.

Fourier-transform infrared spectroscopy (FTIR)

Attenuated total reflection (ATR) infrared spectra are recorded with a Nicolet 6700 spectrometer (Thermo Scientific) equipped with a Golden Gate Standard ZnSe Lenses ATR accessory (SPECAC). Traces are acquired between 4000-600 cm^{-1} at a resolution of 4 cm^{-1}. For each trace, 32 scans are averaged. The spray-dried ACC particles are directly collected on a silicon wafer and analyzed on this substrate while crystal reference samples are placed on the ATR crystals and covered with a silicon wafer.

X-ray diffraction (XRD)

X-ray diffraction traces are acquired using an Empyrean diffractometer (PANalytical) equipped with a PIXcel-1D detector using a Cu Kα radiation source with a wavelength of 1.5405 Å. To maximize the signal to noise ratio, traces are acquired at a grazing incident angle of 1°. The diffraction patterns are collected within a 2θ range of 15 to 50° and at a scanning rate of 0.1 °·s^{-1}. For these measurements, samples are deposited on a one-side polished silicon water.

X-ray photoelectron spectroscopy (XPS)

X-ray photoelectron spectroscopy measurements are carried out using a PHI VersaProbe II scanning XPS microprobe (Physical Electronics) with monochromatic Al Kα X-ray source operated at 24.8 W. The beam size of the X-ray source is 100 µm. For these measurements, samples are deposited onto a silicon wafer that is coated with 20 nm platinum film to avoid any oxygen contribution from the substrate. Data is analyzed using CasaXPS software. All the binding energies are normalized to the carbon 1s peak at 285eV.[81]

X-ray absorption spectroscopy (XAS)

All the XAS experiments are performed at the PHOENIX undulator beamline from the Swiss Light Source (Paul Scherrer Institut, Villigen, Switzerland), which provides photons in the tender X-ray region (0.8 to 8 keV). The size of incident photon beam is 1 mm × 1 mm. For the measurements, the spray-dried ACC particles are directly deposited onto carbon-coated copper TEM grids. The XAS spectra are acquired in total fluorescence mode using a single element silicon drift diode (Ketek GmbH, Germany). As the samples are monolayers of particles, there are no self-absorption effects that usually distort the fluorescence spectra in thick samples. The reference samples are deposited onto a conductive carbon tape glued on a copper plate. The spectra are acquired in the total electron yield mode, which is self-absorption free. All the obtained XAS spectra are corrected by measuring the incident photon flux with a nickel-coated polyester foil that is placed in front of samples and in the beam. The XANES spectra are normalized using the Demeter software.[82] The EXAFS spectra are measured up to k = 10 Å^{-1} with a step size of 0.05 Å^{-1}. The resistive heating system (ISOHEAT Mil Heating Systems GmbH, Germany) is used to vary the temperature *in situ* in XAS measurements. The temperature is monitored using a Pt100 resistive sensor connected to the sample holder.

Atomic force microscopy (AFM)

Atomic force microscopy measurements are conducted in ambient conditions in amplitude modulation mode on a Cypher S system (Asylum Research/Oxford Instruments). The sensitivity of the cantilevers (AC240TS, Olympus) and their spring constant are calibrated using the built-in GetReal™ Automated Probe Calibration procedure. The cantilevers are driven acoustically. The values of the free amplitude are in the range 10-20 nm, with a relative set-point amplitude of 75 %. The scan rates are in the range 3 – 5 Hz. The ACC particles are directly deposited onto carbon-coated copper TEM grids. Image analysis is performed in Gwyddion[83] (http://gwyddion.net/) and power spectral density function (PSDF) is calculated using the built-in function. Power spectral density function is a Fourier transform of the autocorrelation function and represents the contributions of different spatial length scales to the fluctuations in the topography. It therefore provides a global evaluation of the surface roughness of the particles. To avoid the artifacts caused by the background, the PSDF analysis are conducted on an inscribed rectangular region of the surface of each nanoparticle.

Transmission electron microscopy (TEM)

Transmission electron microscopy is conducted on a field emission Talos (FEI) using an acceleration voltage of 200 kV. The condenser aperture 1 is 2000 µm and the condenser aperture 2 is 100 µm. The ACC particles are directly sprayed to carbon film-coated copper or molybdenum grids. Unless specified otherwise, the dose of electrons is kept constant at 60 e·Å^{-2}·s^{-1} and the magnification is kept constant at 190,000 x. To investigate the stability of ACC particles against electron beam-induced decomposition, we increase the electron dose to 400 e·Å^{-2}·s^{-1}. SAED patterns are collected using a 10 µm aperture.

ASSOCIATED CONTENT

Supporting Information

Figure S1-S7, Movie S1-S2 and the calculations of the drying time of drops as well as the quantification of the degree of hydration of ACC particles from XPS results are presented in the Supporting Information. The Supporting Information is available free of charge on the ACS Publications website.

AUTHOR INFORMATION

Corresponding Author

* esther.amstad@epfl.ch

Notes

The authors declare no competing financial interests.

ACKNOWLEDGMENT

We thank Dr. Matthias Kellermeier, Prof. Stephan E. Wolf, Prof. Derk Joester, and Prof. Lia Addadi for the fruitful discussions. We thank Dr. Reuben Yeo, Dr. Pierre Mettraux, and Dr. Thomas La Grange for their help on the characterizations. We acknowledge the Swiss Light Source, Paul Scherrer Institut, Villigen, Switzerland for provision of synchrotron radiation beamtime at PHOENIX beamline and would like to thank Jacinta Moraa Xto, Dr. Katja Henzler for their assistance. This work was financially supported by the Swiss National Center of Competence in Research (NCCR) Bio-Inspired Materials.

REFERENCES

(1) Lackner, K. S. A Guide to CO_2 Sequestration. *Science (80-.).* **2003**, *300* (5626), 1677–1678.

(2) Kleypas, J. A.; Buddemeier, R. W.; Archer, D.; Gattuso, J. P.; Langdon, C.; Opdyke, B. N. Geochemical Consequences of Increased Atmospheric Carbon Dioxide on Coral Reefs. *Science (80-.).* **1999**, *284* (5411), 118–120.

(3) Aizenberg, J.; Lambert, G.; Weiner, S.; Addadi, L. Factors Involved in the Formation of Amorphous and Crystalline Calcium Carbonate: A Study of an Ascidian Skeleton. *J. Am. Chem. Soc.* **2002**, *124* (1), 32–39.

(4) Addadi, L.; Joester, D.; Nudelman, F.; Weiner, S. Mollusk Shell Formation: A Source of New Concepts for Understanding Biomineralization Processes. *Chem. - A Eur. J.* **2006**, *12* (4), 980–987.

(5) Gower, L. B. Biomimetic Model Systems for Investigating the Amorphous Precursor Pathway and Its Role in Biomineralization. *Chem. Rev.* **2008**, *108* (11), 4551–4627.

(6) Wang, J.; Cheng, Q.; Tang, Z. Layered Nanocomposites Inspired by the Structure and Mechanical Properties of Nacre. *Chem. Soc. Rev.* **2012**, *41* (3), 1111–1129.

(7) Sundar, V. C.; Yablon, A. D.; Grazul, J. L.; Ilan, M.; Aizenberg, J. Fibre-Optical Features of a Glass Sponge. *Nature* **2003**, *424* (6951), 899–900.

(8) Meldrum, F. C. Calcium Carbonate in Biomineralisation and Biomimetic Chemistry. *Int. Mater. Rev.* **2003**, *48* (3), 187–224.

(9) Tao, J.; Nielsen, M. H.; De Yoreo, J. J. Nucleation and Phase Transformation Pathways in Electrolyte Solutions Investigated by in Situ Microscopy Techniques. *Curr. Opin. Colloid Interface Sci.* **2018**, *34*, 74–88.

(10) Beniash, E.; Aizenberg, J.; Addadi, L.; Weiner, S. Amorphous Calcium Carbonate Transforms into Calcite during Sea Urchin Larval Spicule Growth. *Proc. R. Soc. B Biol. Sci.* **1997**, *264* (1380), 461–465.

(11) Gower, L. B.; Odom, D. J. Deposition of Calcium Carbonate Films by a Polymer-Induced Liquid-Precursor (PILP) Process. *J. Cryst. Growth* **2000**, *210* (4), 719–734.

(12) Niederberger, M.; Cölfen, H. Oriented Attachment and Mesocrystals: Non-Classical Crystallization Mechanisms Based on Nanoparticle Assembly. *Phys. Chem. Chem. Phys.* **2006**, *8* (28), 3271–3287.

(13) Gebauer, D.; Völkel, A.; Cölfen, H. Stable Prenucleation Calcium Carbonate Clusters. *Science (80-.).* **2008**, *322* (5909), 1819–1822.

(14) Addadi, L.; Raz, S.; Weiner, S. Taking Advantage of Disorder: Amorphous Calcium Carbonate and Its Roles in Biomineralization. *Adv. Mater.* **2003**, *15* (12), 959–970.

(15) Nudelman, F.; Sommerdijk, N. A. J. M. Biomineralization as an Inspiration for Materials Chemistry. *Angew. Chemie - Int. Ed.* **2012**, *51* (27), 6582–6596.

(16) Yao, H. Bin; Ge, J.; Mao, L. B.; Yan, Y. X.; Yu, S. H. 25th Anniversary Article: Artificial Carbonate Nanocrystals and Layered Structural Nanocomposites Inspired by Nacre: Synthesis, Fabrication and Applications. *Adv. Mater.* **2014**, *26* (1), 163–188.

(17) Politi, Y.; Arad, T.; Klein, E.; Weiner, S.; Addadi, L. Sea Urchin Spine Calcite Forms via a Transient Amorphous Calcium Carbonate Phase. *Science (80-.).* **2004**, *306* (5699), 1161–1164.

(18) Politi, Y.; Metzler, R. A.; Abrecht, M.; Gilbert, B.; Wilt, F. H.; Sagi, I.; Addadi, L.; Weiner, S.; Gilbert, P. U. P. A. Transformation Mechanism of Amorphous Calcium Carbonate into Calcite in the Sea Urchin Larval Spicule. *Proc. Natl. Acad. Sci.* **2008**, *105* (45), 17362–17366.

(19) Gower, L. B. Biomimetic Model Systems for Investigating the Amorphous Precursor Pathway and Its Role in Biomineralization. *Chemical Reviews*. ACS Publications 2008, pp 4551–4627.

(20) Weiner, S. STRUCTURAL BIOLOGY: Choosing the Crystallization Path Less Traveled. *Science (80-.).* **2005**, *309* (5737), 1027–1028.

(21) Rodriguez-Navarro, C.; Kudłacz, K.; Cizer, Ö.; Ruiz-Agudo, E. Formation of Amorphous Calcium Carbonate and Its Transformation into Mesostructured Calcite. *CrystEngComm* **2015**, *17* (1), 58–72.

(22) Pontoni, D.; Bolze, J.; Dingenouts, N.; Narayanan, T.; Ballauff, M. Crystallization of Calcium Carbonate Observed In-Situ by Combined Small- and Wide-Angle X-Ray Scattering. *J. Phys. Chem. B* **2003**, *107* (22), 5123–5125.

(23) Bots, P.; Benning, L. G.; Rodriguez-Blanco, J.-D.; Roncal-Herrero, T.; Shaw, S. Mechanistic Insights into the Crystallization of Amorphous Calcium Carbonate (ACC). *Cryst. Growth Des.* **2012**, *12* (7), 3806–3814.

(24) Rieger, J.; Thieme, J.; Schmidt, C. Study of Precipitation Reactions by X-Ray Microscopy: $CaCO_3$ Precipitation and the Effect of Polycarboxylates. *Langmuir* **2000**, *16* (22), 8300–8305.

(25) Raiteri, P.; Gale, J. D. Water Is the Key to Nonclassical Nucleation of Amorphous Calcium Carbonate. *J. Am. Chem. Soc.* **2010**, *132* (49), 17623–17634.

(26) Schmidt, M. P.; Ilott, A. J.; Phillips, B. L.; Reeder, R. J. Structural Changes upon Dehydration of Amorphous Calcium Carbonate. *Cryst. Growth Des.* **2014**, *14* (3), 938–951.

(27) Yoshino, T.; Maruyama, K.; Kagi, H.; Nara, M.; Kim, J. C. Pressure-Induced Crystallization from Amorphous Calcium Carbonate. *Cryst. Growth Des.* **2012**, *12* (7), 3357–3361.

(28) Cartwright, J. H. E.; Checa, A. G.; Gale, J. D.; Gebauer, D.; Sainz-Díaz, C. I. Calcium Carbonate Polyamorphism and Its Role in Biomineralization: How Many Amorphous Calcium Carbonates Are There? *Angew. Chemie Int. Ed.* **2012**, *51* (48), 11960–11970.

(29) Rieger, J.; Kellermeier, M.; Nicoleau, L. Formation of Nanoparticles and Nanostructures-An Industrial Perspective on $CaCO_3$, Cement, and Polymers. *Angew. Chemie Int. Ed.* **2014**, *53* (46), n/a-n/a.

(30) Koga, N.; Nakagoe, Y.; Tanaka, H. Crystallization of Amorphous Calcium Carbonate. *Thermochim. Acta* **1998**, *318* (1–2), 239–244.

(31) Farhadi-Khouzani, M.; Chevrier, D. M.; Zhang, P.; Hedin, N.; Gebauer, D. Water as the Key to Proto-Aragonite Amorphous $CaCO_3$. *Angew. Chemie - Int. Ed.* **2016**, *55* (28), 8117–8120.

(32) Ihli, J.; Kulak, A. N.; Meldrum, F. C. Freeze-Drying Yields Stable and Pure Amorphous Calcium Carbonate (ACC). *Chem. Commun.* **2013**, *49* (30), 3134.

(33) Gebauer, D.; Gunawidjaja, P. N.; Ko, J. Y. P.; Bacsik, Z.; Aziz, B.; Liu, L.; Hu, Y.; Bergström, L.; Tai, C. W.; Sham, T. K.; et al. Proto-Calcite and Proto-Vaterite in Amorphous Calcium Carbonates. *Angew. Chemie - Int. Ed.* **2010**, *49* (47), 8889–8891.

(34) Radha, A. V.; Forbes, T. Z.; Killian, C. E.; Gilbert, P. U. P. A.; Navrotsky, A. Transformation and Crystallization Energetics of Synthetic and Biogenic Amorphous Calcium Carbonate. *Proc. Natl. Acad. Sci.* **2010**, *107* (38), 16438–16443.

(35) Demichelis, R.; Raiteri, P.; Gale, J. D.; Quigley, D.; Gebauer, D. Stable Prenucleation Mineral Clusters Are Liquid-like Ionic Polymers. *Nat. Commun.* **2011**, *2* (1), 590.

(36) Ihli, J.; Wong, W. C.; Noel, E. H.; Kim, Y. Y.; Kulak, A. N.; Christenson, H. K.; Duer, M. J.; Meldrum, F. C. Dehydration and

Crystallization of Amorphous Calcium Carbonate in Solution and in Air. *Nat. Commun.* **2014**, *5*.

(37) Sand, K. K.; Yang, M.; Makovicky, E.; Cooke, D. J.; Hassenkam, T.; Bechgaard, K.; Stipp, S. L. S. Binding of Ethanol on Calcite: The Role of the OH Bond and Its Relevance to Biomineralization. *Langmuir* **2010**, *26* (19), 15239–15247.

(38) Farhadi Khouzani, M.; Chevrier, D. M.; Güttlein, P.; Hauser, K.; Zhang, P.; Hedin, N.; Gebauer, D. Disordered Amorphous Calcium Carbonate from Direct Precipitation. *CrystEngComm* **2015**, *17* (26), 4842–4849.

(39) Chen, S.-F.; Cölfen, H.; Antonietti, M.; Yu, S.-H. Ethanol Assisted Synthesis of Pure and Stable Amorphous Calcium Carbonate Nanoparticles. *Chem. Commun.* **2013**, *49* (83), 9564.

(40) Sand, K. K.; Rodriguez-Blanco, J. D.; Makovicky, E.; Benning, L. G.; Stipp, S. L. S. Crystallization of $CaCO_3$ in Water–Alcohol Mixtures: Spherulitic Growth, Polymorph Stabilization, and Morphology Change. *Cryst. Growth Des.* **2012**, *12* (2), 842–853.

(41) Smeets, P. J. M.; Cho, K. R.; Kempen, R. G. E.; Sommerdijk, N. A. J. M.; De Yoreo, J. J. Calcium Carbonate Nucleation Driven by Ion Binding in a Biomimetic Matrix Revealed by in Situ Electron Microscopy. *Nat. Mater.* **2015**, *14* (4), 394–399.

(42) Dey, A.; de With, G.; Sommerdijk, N. A. J. M. In Situ Techniques in Biomimetic Mineralization Studies of Calcium Carbonate. *Chem. Soc. Rev.* **2010**, *39* (2), 397–409.

(43) Nielsen, M. H.; Aloni, S.; De Yoreo, J. J. In Situ TEM Imaging of $CaCO_3$ Nucleation Reveals Coexistence of Direct and Indirect Pathways. *Science (80-.).* **2014**, *345* (6201), 1158–1162.

(44) Pichon, B. P.; Bomans, P. H. H.; Frederik, P. M.; Sommerdijk, N. A. J. M. A Quasi-Time-Resolved CryoTEM Study of the Nucleation of $CaCO_3$ under Langmuir Monolayers. *J. Am. Chem. Soc.* **2008**, *130* (12), 4034–4040.

(45) Pouget, E. M.; Bomans, P. H. H.; Goos, J. A. C. M.; Frederik, P. M.; De With, G.; Sommerdijk, N. A. J. M. The Initial Stages of Template-Controlled $CaCO_3$ Formation Revealed by Cryo-TEM. *Science (80-.).* **2009**, *323* (5920), 1455–1458.

(46) Rieger, J.; Frechen, T.; Cox, G.; Heckmann, W.; Schmidt, C.; Thieme, J. Precursor Structures in the Crystallization/Precipitation Processes of $CaCO_3$ and Control of Particle Formation by Polyelectrolytes. *Faraday Discuss.* **2007**, *136* (0), 265.

(47) Amstad, E.; Gopinadhan, M.; Holtze, C.; Osuji, C. O.; Brenner, M. P.; Spaepen, F.; Weitz, D. A. Production of Amorphous Nanoparticles by Supersonic Spray-Drying with a Microfluidic Nebulator. *Science (80-.).* **2015**, *349* (6251), 956–960.

(48) Xia, Y.; Whitesides, G. M. SOFT LITHOGRAPHY. *Annu. Rev. Mater. Sci.* **1998**, *28* (1), 153–184.

(49) Loste, E.; Park, R. J.; Warren, J.; Meldrum, F. C. Precipitation of Calcium Carbonate in Confinement. *Adv. Funct. Mater.* **2004**, *14* (12), 1211–1220.

(50) Loste, E.; Wilson, R. M.; Seshadri, R.; Meldrum, F. C. The Role of Magnesium in Stabilising Amorphous Calcium Carbonate and Controlling Calcite Morphologies. *J. Cryst. Growth* **2003**, *254* (1–2), 206–218.

(51) Zou, Z.; Bertinetti, L.; Politi, Y.; Jensen, A. C. S.; Weiner, S.; Addadi, L.; Fratzl, P.; Habraken, W. J. E. M. Opposite Particle Size Effect on Amorphous Calcium Carbonate Crystallization in Water and during Heating in Air. *Chem. Mater.* **2015**, *27* (12), 4237–4246.

(52) Politi, Y.; Levi-Kalisman, Y.; Raz, S.; Wilt, F.; Addadi, L.; Weiner, S.; Sagi, I. Structural Characterization of the Transient Amorphous Calcium Carbonate Precursor Phase in Sea Urchin Embryos. *Adv. Funct. Mater.* **2006**, *16* (10), 1289–1298.

(53) Michel, F. M.; MacDonald, J.; Feng, J.; Phillips, B. L.; Ehm, L.; Tarabrella, C.; Parise, J. B.; Reeder, R. J. Structural Characteristics of Synthetic Amorphous Calcium Carbonate. *Chem. Mater.* **2008**, *20* (14), 4720–4728.

(54) Levi-Kalisman, Y.; Raz, S.; Weiner, S.; Addadi, L.; Sagi, I. Structural Differences Between Biogenic Amorphous Calcium Carbonate Phases Using X-Ray Absorption Spectroscopy. *Adv. Funct. Mater.* **2002**, *12* (1), 43.

(55) Lam, R. S. K.; Charnock, J. M.; Lennie, A.; Meldrum, F. C. Synthesis-Dependant Structural Variations in Amorphous Calcium Carbonate. *CrystEngComm* **2007**, *9* (12), 1226.

(56) Nielsen, M. H.; Aloni, S.; De Yoreo, J. J. In Situ TEM Imaging of $CaCO_3$ Nucleation Reveals Coexistence of Direct and Indirect Pathways. *Science (80-.).* **2014**, *345* (6201), 1158–1162.

(57) Rodriguez-Blanco, J. D.; Shaw, S.; Benning, L. G. How to Make "stable" ACC: Protocol and Preliminary Structural Characterization. *Mineral. Mag.* **2008**, *72* (1), 283–286.

(58) Grogan, J. M.; Schneider, N. M.; Ross, F. M.; Bau, H. H. Bubble and Pattern Formation in Liquid Induced by an Electron Beam. *Nano Lett.* **2014**, *14* (1), 359–364.

(59) Albéric, M.; Bertinetti, L.; Zou, Z.; Fratzl, P.; Habraken, W.; Politi, Y. The Crystallization of Amorphous Calcium Carbonate Is Kinetically Governed by Ion Impurities and Water. *Adv. Sci.* **2018**, *1701000*, 1701000.

(60) Tobler, D. J.; Rodriguez Blanco, J. D.; Sørensen, H. O.; Stipp, S. L. S.; Dideriksen, K. Effect of PH on Amorphous Calcium Carbonate Structure and Transformation. *Cryst. Growth Des.* **2016**, *16* (8), 4500–4508.

(61) Gebauer, D.; Gunawidjaja, P. N.; Ko, J. Y. P.; Bacsik, Z.; Aziz, B.; Liu, L.; Hu, Y.; Bergström, L.; Tai, C.-W.; Sham, T.-K.; et al. Proto-Calcite and Proto-Vaterite in Amorphous Calcium Carbonates. *Angew. Chemie Int. Ed.* **2010**, *49* (47), 8889–8891.

(62) Saharay, M.; Yazaydin, A. O.; Kirkpatrick, R. J. Dehydration-Induced Amorphous Phases of Calcium Carbonate. *J. Phys. Chem. B* **2013**, *117* (12), 3328–3336.

(63) Sen, S.; Kaseman, D. C.; Colas, B.; Jacob, D. E.; Clark, S. M. Hydrogen Bonding Induced Distortion of CO_3 Units and Kinetic Stabilization of Amorphous Calcium Carbonate: Results from 2D ^{13}C NMR Spectroscopy. *Phys. Chem. Chem. Phys.* **2016**, *18* (30), 20330–20337.

(64) Bushuev, Y. G.; Finney, A. R.; Rodger, P. M. Stability and Structure of Hydrated Amorphous Calcium Carbonate. *Cryst. Growth Des.* **2015**, *15* (11), 5269–5279.

(65) Singer, J. W.; Yazaydin, A. Ö.; Kirkpatrick, R. J.; Bowers, G. M. Structure and Transformation of Amorphous Calcium Carbonate: A Solid-State ^{43}Ca NMR and Computational Molecular Dynamics Investigation. *Chem. Mater.* **2012**, *24* (10), 1828–1836.

(66) Goodwin, A. L.; Michel, F. M.; Phillips, B. L.; Keen, D. A.; Dove, M. T.; Reeder, R. J. Nanoporous Structure and Medium-Range Order in Synthetic Amorphous Calcium Carbonate. *Chem. Mater.* **2010**, *22* (10), 3197–3205.

(67) Saharay, M.; Kirkpatrick, R. J. Water Dynamics in Hydrated Amorphous Materials: A Molecular Dynamics Study of the Effects of Dehydration in Amorphous Calcium Carbonate. *Phys. Chem. Chem. Phys.* **2017**, *19* (43), 29594–29600.

(68) Rodriguez-Navarro, C.; Ruiz-Agudo, E.; Luque, A.; Rodriguez-Navarro, A. B.; Ortega-Huertas, M. Thermal Decomposition of Calcite: Mechanisms of Formation and Textural Evolution of CaO Nanocrystals. *Am. Mineral.* **2009**, *94* (4), 578–593.

(69) Gebauer, D.; Cölfen, H.; Verch, A.; Antonietti, M. The Multiple Roles of Additives in $CaCO_3$ Crystallization: A Quantitative Case Study. *Adv. Mater.* **2009**, *21* (4), 435–439.

(70) Verch, A.; Gebauer, D.; Antonietti, M.; Cölfen, H. How to Control the Scaling of $CaCO_3$: A "Fingerprinting Technique" to Classify Additives. *Phys. Chem. Chem. Phys.* **2011**, *13* (37), 16811.

(71) Ihli, J.; Kim, Y.-Y.; Noel, E. H.; Meldrum, F. C. The Effect of Additives on Amorphous Calcium Carbonate (ACC): Janus Behavior in Solution and the Solid State. *Adv. Funct. Mater.* **2013**, *23* (12), 1575–1585.

(72) Xu, X. R.; Cai, A. H.; Liu, R.; Pan, H. H.; Tang, R. K.; Cho, K. The Roles of Water and Polyelectrolytes in the Phase Transformation of Amorphous Calcium Carbonate. *J. Cryst. Growth* **2008**, *310* (16), 3779–3787.

(73) Zou, Z.; Bertinetti, L.; Politi, Y.; Fratzl, P.; Habraken, W. J. E. M. Control of Polymorph Selection in Amorphous Calcium Carbonate Crystallization by Poly(Aspartic Acid): Two Different Mechanisms. *Small* **2017**, *13* (21), 1603100.

(74) Tobler, D. J.; Rodriguez-Blanco, J. D.; Dideriksen, K.; Bovet, N.; Sand, K. K.; Stipp, S. L. S. Citrate Effects on Amorphous

Calcium Carbonate (ACC) Structure, Stability, and Crystallization. *Adv. Funct. Mater.* **2015**, *25* (20), 3081–3090.

(75) Sinn, C. G.; Dimova, R.; Antonietti, M. Isothermal Titration Calorimetry of the Polyelectrolyte/Water Interaction and Binding of Ca^{2+} : Effects Determining the Quality of Polymeric Scale Inhibitors. *Macromolecules* **2004**, *37* (9), 3444–3450.

(76) Kababya, S.; Gal, A.; Kahil, K.; Weiner, S.; Addadi, L.; Schmidt, A. Phosphate-Water Interplay Tunes Amorphous Calcium Carbonate Metastability: Spontaneous Phase Separation and Crystallization Vs Stabilization Viewed by Solid State NMR. *J. Am. Chem. Soc.* **2015**, *137* (2), 990–998.

(77) Tribello, G. A.; Bruneval, F.; Liew, C.; Parrinello, M. A Molecular Dynamics Study of the Early Stages of Calcium Carbonate Growth. *J. Phys. Chem. B* **2009**, *113* (34), 11680–11687.

(78) Raz, S.; Hamilton, P. C.; Wilt, F. H.; Weiner, S.; Addadi, L. The Transient Phase of Amorphous Calcium Carbonate in Sea Urchin Larval Spicules: The Involvement of Proteins and Magnesium Ions in Its Formation and Stabilization. *Adv. Funct. Mater.* **2003**, *13* (6), 480–486.

(79) Nudelman, F.; Sonmezler, E.; Bomans, P. H. H.; de With, G.; Sommerdijk, N. A. J. M. Stabilization of Amorphous Calcium Carbonate by Controlling Its Particle Size. *Nanoscale* **2010**, *2* (11), 2436.

(80) Rodriguez-Blanco, J. D.; Shaw, S.; Benning, L. G. The Kinetics and Mechanisms of Amorphous Calcium Carbonate (ACC) Crystallization to Calcite, Viavaterite. *Nanoscale* **2011**, *3* (1), 265–271.

(81) Ni, M.; Ratner, B. D. Differentiating Calcium Carbonate Polymorphs by Surface Analysis Techniques - An XPS and TOF-SIMS Study. *Surf. Interface Anal.* **2008**, *40* (10), 1356–1361.

(82) Ravel, B.; Newville, M. ATHENA, ARTEMIS, HEPHAESTUS: Data Analysis for X-Ray Absorption Spectroscopy Using IFEFFIT. *J. Synchrotron Radiat.* **2005**, *12* (4), 537–541.

(83) Nečas, D.; Klapetek, P. Gwyddion: An Open-Source Software for SPM Data Analysis. *Open Phys.* **2012**, *10* (1), 181–188.

Amorphous $CaCO_3$: Influence of the formation time on its degree of hydration and stability

Graphic entry for the Table of Contents (TOC)